ELECTRONIC SUPPLEMENTARY INFORMATION (ESI)

Microwave assisted dry-gel conversion - a new sustainable route for the rapid synthesis of metal-organic frameworks with solvent re-use

*Niels Tannert[a], Serkan Gökpinar[a], Emrah Hastürk[a], Sandra Nießing[a] and Christoph Janiak[a]**

*[a] Institut für Anorganische Chemie und Strukturchemie, Heinrich-Heine-Universität Düsseldorf, Universitätsstraße 1, 40225 Düsseldorf, Germany. *E-mail: janiak@uni-duesseldorf.de*

[b] These authors contributed equally.

Keywords
Metal-Organic Frameworks, MIL-100(Fe), UiO-66, MIL-140A, Aluminum fumarate, Microwave, Dry-Gel Conversion, Synthesis Optimization, Sustainability, Solvent re-use

Emails: niels.tannert@hhu.de; serkan.goekpinar@hhu.de; emrah.hastuerk@hhu.de; sandra.niesssing@hhu.de

Table of Contents

S1. Materials and equipment

All chemicals were used as received from supplier (cf. Table S1).

Table S1 *Used chemicals, supplier and purities.*

Chemical	Supplier	Purity
$Al(SO)_4 \cdot 18H_2O$	AppliChem	not specified
Basolite™ A520	Sigma Aldrich	not specified
Basolite™ F300	Sigma Aldrich	not specified
Benzene-1,4-dicarboxylic acid	Sigma Aldrich	≥98.0%
Benzene-1,3,5-tricarboxylic acid	Sigma Aldrich	95%
Benzoic acid	Riedel de Haen	99.5%
Dimethylformamide	Fischer Chemicals	99.99%
Ethanol	Sigma Aldrich	>99.8%
$FeCl_3 \cdot 6H_2O$	Sigma Aldrich	97%
$Fe(NO)_3 \cdot 9H_2O$	Sigma Aldrich	98%
Fumaric acid	Alfa Aesar	99%
Hydrochloric acid, 37%	Sigma Aldrich	p.a.
Hydrofluoric acid, 48%	Sigma Aldrich	p.a.
NaOH (microgranulate)	Chem Solute	not specified
Nitric acid, 65%	VWR Chemicals	p.a.
Sodium fluoride	Sigma Aldrich	99.99%
Tetrabutylammonium fluoride, hydrate	Sigma Aldrich	96%
Zirconium chloride	Alfa Aesar	≥99.5%

Powder X-ray diffraction (PXRD) patterns were obtained out at ambient temperature on a *D2 phaser* (BRUKER, Billerica, US) using Cu-Kα radiation (λ = 1.54182 Å) between 5° < 2Θ < 50° with a scanning rate of 0.0125 °/s (300 W, 30 kV, 10 mA). The diffractograms were obtained on a flat "low background sample holder", in which at low angle the beam spot is strongly broadened so that only a fraction of the reflected radiation reaches the detector, hence the low relative intensities measured at 2Θ < 7°. Analyses of the diffractograms were carried out with *Match 3.11* software.

Thermogravimetric analysis (TGA) was performed with a *TG209 F3 Tarsus* (NETZSCH, Selb, Germany). Samples were placed in alumina pans and heated at a rate of 5 $Kmin^{-1}$ from 25-600 °C under synthetic air atmosphere.

Nitrogen (purity 99.9990%, 5.0) physisorption isotherms were carried out on a *Nova 4000e* (QUANTACHROME, Odelzhausen, Germany) at T = 77 K. Before measuring of the isotherms, the products were transferred into glass tubes capped with septa, which were weighted out before. These tubes were attached to the corresponding degassing port of the sorption analyzer, degassed under vacuum at 120 °C for 3 h, weighted out again and then transferred to the analysis port of the sorption analyzer. BET surface areas were calculated from the N_2 adsorption isotherms in an individual p/p_0 range for each MOF (cf. Section S7). Total pore volumes were calculated from the N_2 sorption isotherm at $p/p_0 = 0.95$. NLDFT calculations for the pore size distribution curves were done with the native *NovaWin 11.03* software using the 'N_2 at 77 K on carbon, slit pore, NLDFT equilibrium' model.

Scanning electron microscopy (SEM) images were recorded with a *JSM-6510LV QSEM Advanced electron microscope* (JEOL, Akishima, Japan) with a LaB_6 cathode at 5–20 keV. The microscope was equipped with a *Xflash 410* (BRUKER, Billerica, US) silicon drift detector.

The microwave for MW-DGC syntheses was a *MARS-5* (CEM, Matthews, US).

DGC inlays were self-built, made of Teflon. The holes in the DGC sieves had 0.5 mm diameter. The ring inlays, shown in Figure S1, can have various heights for adjustment. We thank the precision mechanics workshop of Heinrich-Heine-University.

Figure S1 *Top: Full autoclave set for MW-DGC with microwave tube, lid and screw-cap, three ring inlays for height-adjustment of sieve and DGC sieve, given also at bottom left in close-up view. Bottom right: Close-up view of a CE-DGC sieve with inlay ring for height adjustment.*

S2. Brief description of synthesized metal-organic frameworks

S2.1. MIL-100(Fe)

Metal-organic frameworks with MIL-100 topology (*Matériaux de l'Institut Lavoisier*) were first described by the group of G. Férey in 2004.[1] Figure S2 shows the structural features of MIL-100(Fe) with respect to bonding situations and cavities.

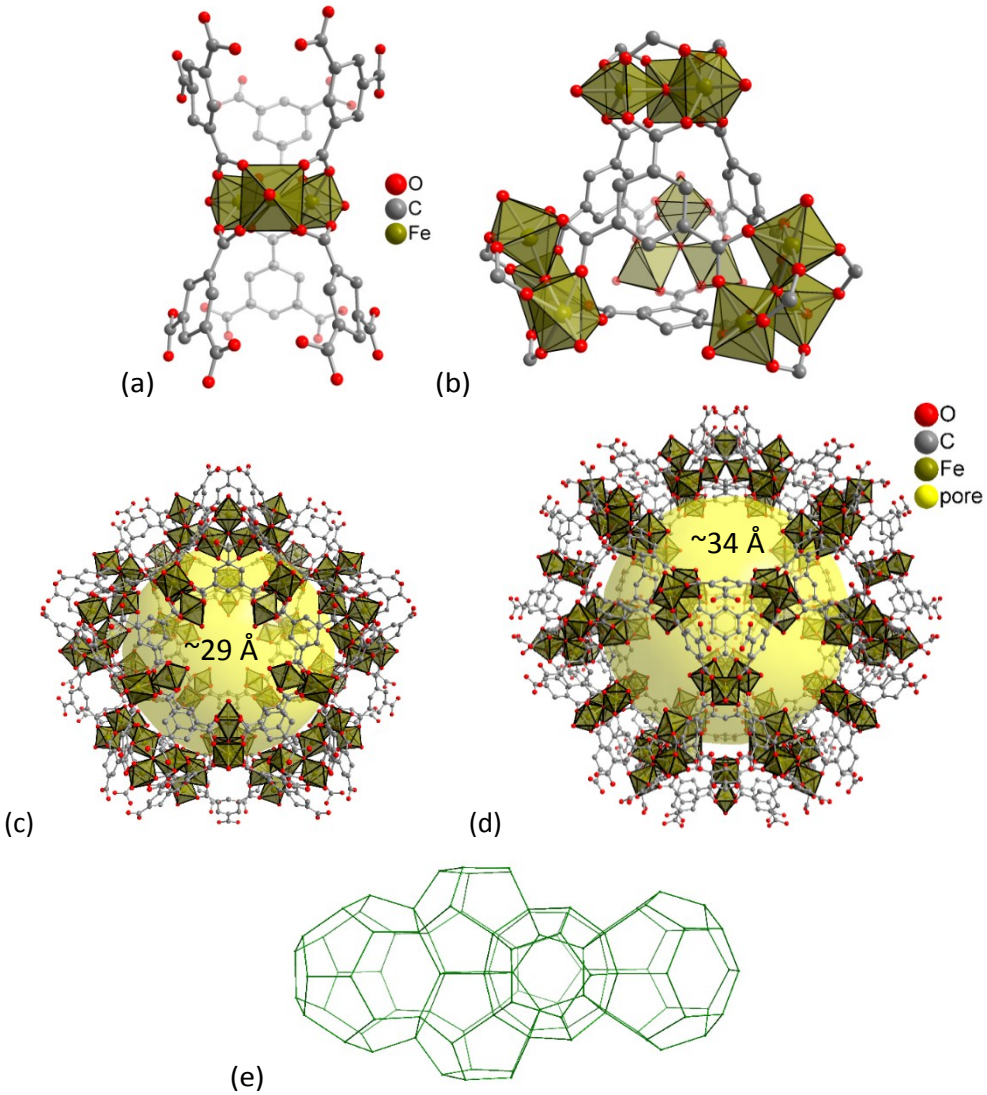

Figure S2 *Structural features of MIL-100(Fe). (a) secondary building unit (SBU), (b) supertetrahedra, (c) small S cage, (d) large L cage and (e) topology of the mesoporous network (objects are not drawn to scale). Hydrogen atoms and solvent molecules are not shown. The yellow spheres in the mesoporous cages with the indicated diameters take into account the van-der-Waals radii of the framework walls. Hydrogen atoms and solvent molecules of crystallization are not shown. Graphics have been drawn with the software DIAMOND [2] from the deposited cif-file under CCDC no. 640536 for Fe.[3]*

MIL-100(Fe) consists of hybrid supertetrahedra with oxocentered trimers of trivalent metal octahedra connected by trimesate anions (benzene-1,3,5-tricarboxylate – short: BTC).[1,4] MIL-100(Fe) with the chemical formula $[Fe^{III}_3(\mu_3\text{-}O)(X)(BTC)_2 \cdot nH_2O]_m$ (with X = F, OH; depending on synthetic conditions) exhibit zeolite MTN topology, mesoporous cages of 25 and 29 Å with microporous (i.e. <2

nm) windows of 5.5 and 8.6 Å and an inner specific surface area of 356-2320 m^2g^{-1} (*Brunauer-Emmett-Teller*, BET area), highly depending on synthetic conditions.[5-6]

MIL-100 is studied for gas storage and sequestration,[11-7,] in composites,[8,9] as sorption material for heating/cooling applications,[10-11,12,13] mixed-matrix membranes,[14] many-sided synthesis optimizations,[5,8,10,15,16] drug delivery and more.[17-18] Notably, MIL-100 materials were shown to be highly versatile and tunable in terms of crystallinity, morphology and particle size.[19-20] This in turn allows their preparation as xerogels and aerogels, what expands applicability even further.[21-22] Moreover, MIL-100 proved to be suitable as heterogeneous catalyst in several organic reactions.[3,20,22,23-24] Low toxicity, biocompatibility and abundancy of iron are key-factors for utilization of MIL-100(Fe) in application-oriented research.[3]

MIL-100(Fe) can as well be prepared continuously with a space-time yield (STY) of 20 kg m^{-3} day^{-1}.[25] STY is hereby defined as the amount of produced MOF (kg) per unit volume of reactor (m^3) per day of synthesis (alternatively: per unit volume of reaction mixture (m^3) per day of synthesis [26]).[27]

Exemplarily, Figure S3 depicts MIL-100(Fe) products, obtained by DGC.

Figure S3 *Left: Autoclave with DGC sieve, with MIL-100(Fe) product on top. Right: Products obtained from* $Fe(NO_3)_3 \cdot 9H_2O$ *(left),* $FeCl_3 \cdot 6H_2O$ *(right).*

S2.2. UiO-66 and MIL-140A

Zirconium MOFs represent a subclass of frameworks, which gets more and more attention, due to their excellent stability in thermal, aqueous and acid conditions.[28,29] Among these Zr-MOFs is UiO-66 (*Universitetet i Oslo*), which was first synthesized by Lillerud and co-workers[30] and MIL-140A synthesized by Serre and co-workers.[31] UiO-MOFs have a $\{Zr_6O_4(OH)_4\}$-SBU, which is an octahedral Zr_6-cluster of six edge-sharing ZrO_8 square-antiprism and which is 12 coordinated by the linker molecules to 12 neighboring SBUs in a face-centered cubic (fcc) packing arrangement.[44] Depending on used dicarboxylate linker it can be obtained UiO-66 (linker = 1,4-benzenedicarboxylic acid), UiO-67 (linker = 4,4'-biphenyldicarboxylic acid) or UiO-68 (4,4''-terphenyldicarboxylic acid) with an isoreticular framework. Figure S4 shows the crystal structure of zirconium terephthalate UiO-66.

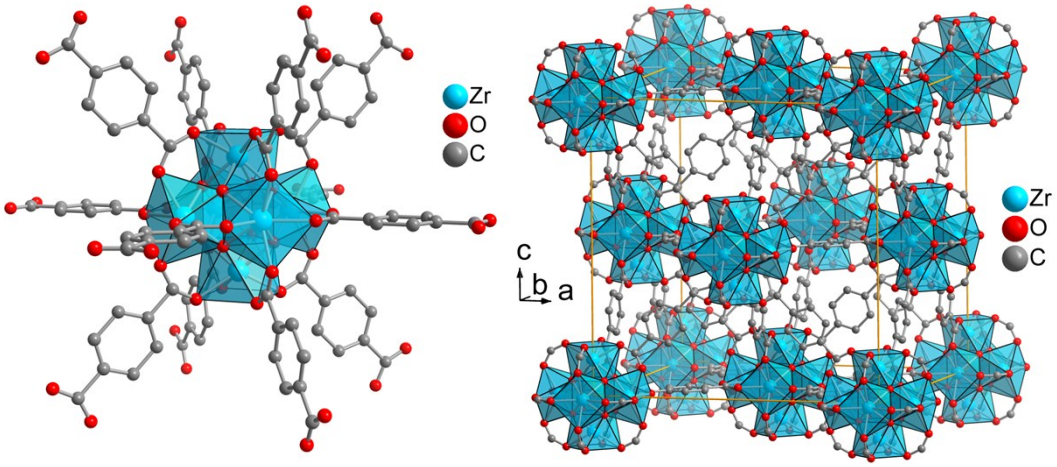

Figure S4 *Crystal structure of zirconium terephthalate UiO-66.[44] Hydrogen atoms and solvent molecules are not shown. The UiO-66 structure is drawn with the software Diamond [2] from the deposited cif-file under CCDC no. 837796.[32]*

The properties of these UiO-MOFs are interesting for gas storage,[33] separation,[34] water sorption,[35,36] sensing[37] and catalysis.[38,39] UiO-66 can be synthesized solvothermally, *via* mechanochemistry[40] or DGC[41] and also continuously with a space-time yield (STY) of 4,899 kg d^{-1} m^{-3}.[42]

Figure S5 shows the crystal structure of zirconium terephthalate MIL-140A. The MIL-140 series are polymorphs of the UiOs with the general formula [ZrO(linker)], while MIL-140A has a BDC linker. MIL-140s consist of one dimensional zirconium oxide chains (along the c-axis), which are linked to six other chains through dicarboxylate linkers, thereby obstructing one-dimensional channels.[45]

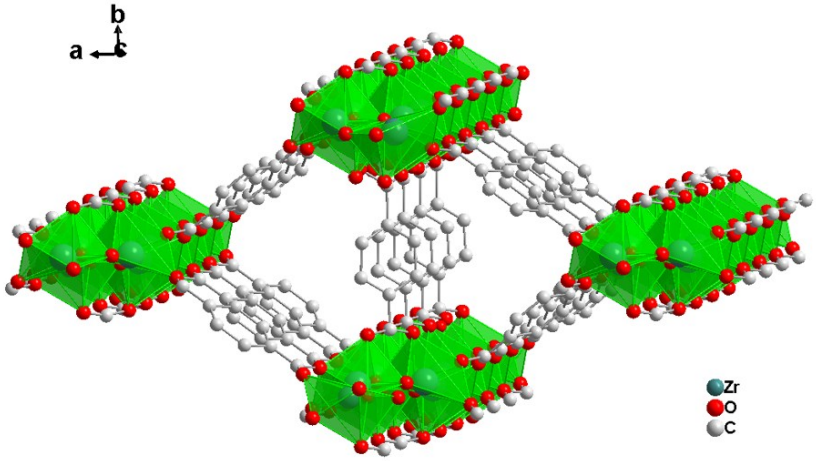

Figure S5 *Crystal structure of zirconium terephthalate MIL-140A. The MIL-140A structure is drawn with the software Diamond [2] from the deposited cif-file under CCDC no. 905026.[45]*

S2.3. Aluminum fumarate (Alfum)

Aluminum fumarate (Alfum) was first described in the patent literature.[43,44] Figure S6 shows the structural features of aluminum fumarate with respect to bonding situations and cavities.

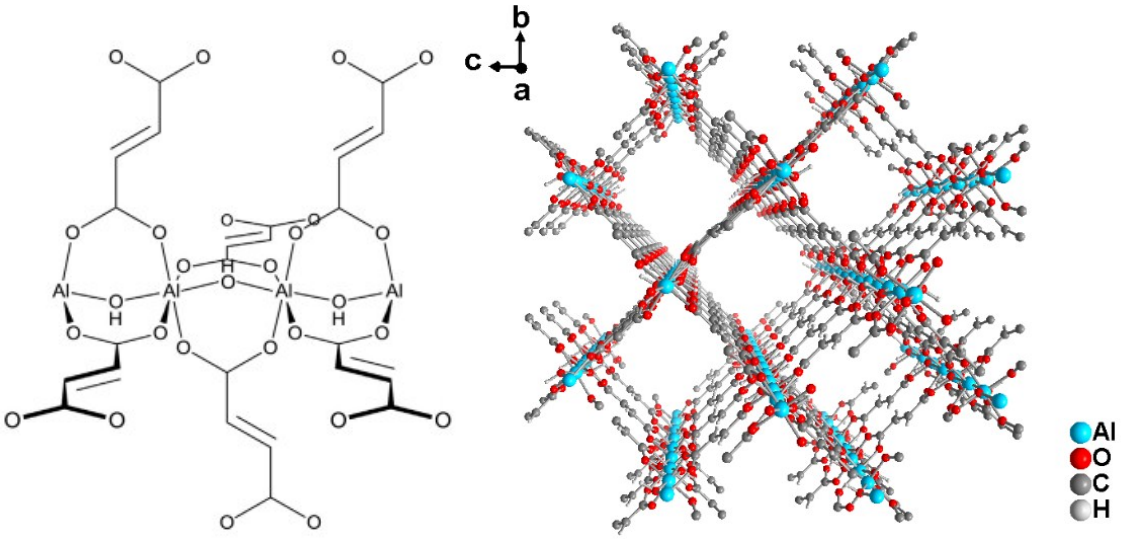

Figure S6 *Left: Building block of Alfum, in analogy to the structure of MIL-53. The illustration was taken from ref. [45] Right: Crystal structure of aluminum fumarate. Graphic produced by software Diamond [2] from cif-file for Basolite A520 (CSD-Refcode DOYBEA, CCDC no. 1051975).[46]*

Alfum resembles the monoclinic MIL-53(Al) structure (i.e. with benzene-1,4-dicarboxylate as linker) with infinite Al-OH-Al chains connected by fumarate linkers. It has the chemical formula $[Al(OH)(O_2C\text{-}CH{=}CH\text{-}CO_2)]_n$ and displays microporous, rhombohedral channels with circa 5.7 x 6.0 Å^2 free dimensions.[60,47]

Aluminum fumarate is one of the most promising MOFs for application,[59,60,48] due to its hydrothermal stability and an environmentally friendly synthesis route with water as single solvent, inexpensive and benign metal cation, moreover, a "green" linker from renewable biomass,[49] besides possible large scale production with a high STY of >3615 kg m^{-3} day^{-1}.[57,58,50] Gaab *et al.* proved its applicability as storage container for natural gas, used as fuel in a vehicle, by 40% increased cruising distance.[64] Moreover, Alfum was proven to represent suitable water sorption characteristics and cyclic stability for heat transformation application,[59] it is applicable as super adsorbent for removal of fluoride from water [51] and in desalination processes [52] and it was proposed to be the best porous solid for mechanical energy storage.[53] It can as well be prepared *via* (potentially continuously operable) mechanochemical techniques, such as extrusion.[54] Thereby, 27000 kg m^{-3} day^{-1} STY were calculated to be feasible.[55] Continuous flow methods achieved even STYs up to 97 159 kg m^{-3} day^{-1} at 5.6 kg h^{-1} and ca. 1000-1100 m^{2}g^{-1}.[40]

S3. Syntheses of MIL-100(Fe)

In a typical synthetic procedure, the metal salts $Fe(NO)_3 \cdot 9H_2O$ and $FeCl_3 \cdot 6H_2O$ were ground with H_3BTC in a molar ratio of 1:1 (2-4 mmol of each reactant) *via* ball-milling (20 Hz, 20 Min) using a *Retsch MM301* (RETSCH, Haan, Germany). However, simple grinding in a mortar yielded the desired phase too.

S3.1. Microwave-assisted dry-gel conversion (MW-DGC)

The precursor mixture of around 100 mg combined mass was placed on a MW-DGC sieve (cf. Fig. S1) with water or acidic solutions (5 mL) at the bottom of the Teflon-reactor, which was tightly closed and heated to 150 °C for 180 min by applying 800 W, using a *CEM MARS-5* microwave. The orange-brownish (from $Fe(NO)_3 \cdot 9H_2O$) or reddish (from $FeCl_3 \cdot 6H_2O$) solid products were washed with water and ethanol three times (10 mL each) and dried (80 °C, 24 h). Amounts of starting materials and yields in already optimized syntheses are given in Table S2.

Table S2 *Synthesis details of different MIL-100(Fe) samples obtained via MW-DGC.*

Fe source	Solvent (5 mL)	$m_{Fe\text{-}salt}$ [mg]	m_{H3BTC} [mg]	$n_{Fe} = n_{BTC}$ [mmol]	Yield [g]	Yield [%] [a]	BET [m^2g^{-1}]
Fe-chloride	neat H_2O	50.0	38.9	0.185	0.045	78	1002
	H_2O + HNO_3 (1:1)	49.5	38.4	0.183	0.046	81	460
	H_2O/EtOH (4:1)	53.0	41.2	0.196	0.037	61	922
Fe-nitrate	neat H_2O	77.2	40.1	0.191	0.047	81	1105
	H_2O + HNO_3 (1:1)	78.0	41.3	0.193	0.046	78	526
	H_2O/EtOH (4:1)	84.8	45.0	0.210	0.050	78	1180

[a] Based on the amount of Fe-salt and on the MIL-100(Fe) formula of $[Fe^{III}_3(\mu_3\text{-}O)(H_2O)_2(Cl)(BTC)_2 \cdot 14.5\ H_2O]_m$ and M_W= 930.47 $gmol^{-1}$ for MIL-100(Fe) products of Fe-chloride based synthesis, respectively $[Fe^{III}_3(\mu_3\text{-}O)(H_2O)_2(OH)(BTC)_2 \cdot 14.5\ H_2O]_m$ and M_W = 912.02 $gmol^{-1}$ for MIL-100(Fe) products of Fe-nitrate based synthesis. The amount of crystal water after drying was estimated to be x = 14.5 per formula unit in accordance to earlier reports.[9,11]

S3.2. Conventionally heated dry-gel conversion (CE-DGC)

Synthetic conversions of precursors were performed on top of a DGC sieve holder with water or acidic solutions (20 mL) on the bottom of a Teflon-lined steel autoclave at 150 °C (2 h heating to 150 °C, 24 h, 2 h cooling) using electrical heating ovens. The orange-brownish (from $Fe(NO)_3 \cdot 9H_2O$) or reddish (from $FeCl_3 \cdot 6H_2O$) solid products were washed with water and ethanol three times (each 40 mL), dried and finally activated (80 °C, 24 h). Initial weights of precursor mixtures and yields in already optimized syntheses are given in Table S3.

Table S3 *Synthesis details of different MIL-100(Fe) samples obtained via CE-DGC.*

Fe source	Solvent (20 mL)	$m_{Fe\text{-}salt}$ [mg]	m_{H3BTC} [mg]	$n_{Fe} = n_{BTC}$ [mmol]	Yield [g]	Yield [%] [a]	BET [m^2g^{-1}]
Fe-chloride	neat H_2O	205.4	159.7	0.760	0.162	69	1776
	H_2O + HNO_3 (1:1)	203.8	158.4	0.754	0.146	62	1469
	H_2O/EtOH (4:1)	197.0	153.2	0.729	0.101	45	1287
Fe-nitrate	neat H_2O	444.0	230.9	1.099	0.267	80	1876
	H_2O + HNO_3 (1:1)	248.0	129.0	0.614	0.166	89	1550
	H_2O/EtOH (4:1)	190.7	99.2	0.472	0.138	96	1561

[a] Based on the amount of Fe-salt and on the MIL-100(Fe) formula of $[Fe^{III}_3(\mu_3\text{-}O)(H_2O)_2(Cl)(BTC)_2 \cdot 14.5\ H_2O]_m$ and M_W= 930.47 $gmol^{-1}$ for MIL-100(Fe) products of

Fe-chloride based synthesis, respectively $[Fe^{III}_3(\mu_3\text{-}O)(H_2O)_2(OH)(BTC)_2 \cdot 14.5\ H_2O]_m$ and $M_W = 912.02\ gmol^{-1}$ for MIL-100(Fe) products of Fe-nitrate based synthesis. The amount of crystal water after drying was estimated to be x = 14.5 per formula unit in accordance to earlier reports.[9,11]

During our work we have carried out synthesis optimization for the MW-DGC approach for MIL-100(Fe): We varied the molar ratio of reactants, reaction time and temperature, respectively microwave irradiation power. Additionally, we performed syntheses with fluoride sources such as tetrabutylammonium fluoride (TBAF) and sodium fluoride, by adding 2 wt.% to the precursor mixture. Aqueous HF was added to the solvent (1: 10 by vol.). The addition of any fluoride source did not lead to improved products. Also other ratios of water/ethanol and water/HNO_3 were applied, but did not yield improved products. Thus, we describe only the optimized syntheses above.

S4. Syntheses of UiO-66 and MIL-140A

S4.1. UiO-66

S4.1.1. Microwave-assisted dry-gel conversion (MW-DGC)

For the synthesis of UiO-66-HCl *via* MW-DGC, $ZrCl_4$ (88 mg, 0.38 mmol, 1.0 eq), H_2BDC (63 mg, 0.38 mmol, 1.0 eq) and benzoic acid (BA) (100 mg, 0.82 mmol, 2.1 eq) were mixed, ground in a mortar and placed on the sieve. DMF solvent (10 mL) and 1 mL of HCl (37%) was placed at the bottom of the Teflon tube. The sieve, which was filled with precursor mixture was placed above the solvent-mixture and the Teflon tube was capped and heated to 180 °C (10 min heating to 180 °C, 50 min, cooling) by applying 600 W, using a *CEM MARS-5* microwave. After the tube was cooled down to room temperature, the obtained as-synthesized product was soaked in DMF (2 x 5 mL, 24 h each) and ethanol (5 mL, 24 h). The solvent was exchanged every 24 h. After a total time of 3 d of soaking, the solids were centrifuged and dried under vacuum. For UiO-66-IL a DMF/$[BMIm]NTf_2$ (9:1 by vol.) solvent mixture was used.

S4.1.2. Synthesis of ionic liquid (IL) $[BMIm]NTf_2$

The ionic liquid was synthesized according to a modified procedure of Deetlefs *et al.*.[56] For microwave synthesis of [BMIm]Cl a mixture of 1-methylimidazole (150 mmol) and 1-chlorobutane (153 mmol) was placed in a Teflon vessel equipped with a magnetic stirrer. The temperature was raised to 160 °C over the course of 20 min, and microwave irradiation continued for a further 60 min. The anion of [BMIm]Cl was exchanged by reaction with $LiNTf_2$ (150 mmol) in H_2O to give the $[BMIm]NTf_2$ according to the procedure by Wegner *et al.*.[57]

S4.2. MIL-140A

S4.2.1. Microwave-assisted dry-gel conversion (MW-DGC)

For the synthesis of MIL-140A *via* MW-DGC, $ZrCl_4$ (88 mg, 0.38 mmol, 1 eq), H_2BDC (63 mg, 0.38 mmol, 1 eq) and benzoic acid (100 mg, 0.82 mmol, 2.1 eq) were mixed, ground in a mortar and placed on the sieve. The DMF solvent (10 mL) was placed at the bottom of the Teflon tube and the sieve, filled with precursor mixture, was placed above the solvent. The Teflon tube was capped and heated to 160 °C (10 min heating to 160 °C, 80 min, cooling) by applying 600 W, using a *CEM MARS-5* microwave. After the tube was cooled down to room temperature, the obtained as-synthesized product was soaked in DMF (2 x 5 mL, 24 h each) and ethanol (5 mL, 24 h). The solvent was exchanged every 24 h. After 3 d of soaking, the solids were centrifuged and dried under vacuum.

Yields, BET areas and pore volumes for UiO-66 and MIL-140A from MW-DGC synthesis are given in Table 2 in the full manuscript, in comparison with literature values for CE-DGC and solution synthesis.

S5. Syntheses of aluminum fumarate

The compounds $Al_2(SO_4)_3 \cdot 18H_2O$, fumaric acid and NaOH were mixed at a molar ratio of 1:2:4 by rapid grinding in a mortar. Thereupon, the precursor mixture was quickly placed on top of a DGC sieve holder, quickly placed in the Teflon container for the reaction in the microwave or CE oven.

S5.1. Microwave-assisted dry-gel conversion (MW-DGC)

Synthetic conversions of precursors were performed on top of a MW-DGC sieve holder with water (5 mL) at the bottom of a Teflon-reactor at 100 °C (60 Min) by applying 800 W using a *CEM MARS-5* microwave. The white products were washed three times with water (10 mL each), and dried under vacuum (80 °C, 24 h). Initial weights of precursor mixtures and yields are given in Table S4.

Table S4 *Synthesis details of different aluminum fumarate samples obtained via repeated MW-DGC.*

Precursor [g]	$m_{Al\text{-}salt}$ [g]	$m_{fumaric\ acid}$ [g]	n_{Al} [mmol]	$n_{fumaric\ acid}$ [mmol]	Yield [g]	Yield [%] [a]	BET [m^2g^{-1}]
0.273	0.172	0.060	0.52	0.52	0.062	76	1075
0.252	0.159	0.055	0.48	0.48	0.060	81	1150
0.298	0.188	0.065	0.56	0.56	0.079	89	1128

[a] Based on the amount of Al-salt and on the product formula $[Al(OH)(O_2C\text{-}CH{=}CH\text{-}CO_2)]_n$ and M_W = 158.045 $gmol^{-1}$ for Alfum.

S5.2. Conventionally electric-heated dry-gel conversion (CE-DGC)

Synthetic conversions of precursors were performed on top of a DGC sieve holder with water (2 mL) at the bottom of a Teflon-reactor inside a stainless-steel autoclave at 100 °C (6-24 h) in an electrically heated oven. The white products were washed three times with water (50 mL each) and dried under vacuum (80 °C, 24 h). Initial weights of aluminum sulfate and yields are given in Table S5.

Table S5 *Synthesis details of different aluminum fumarate samples obtained via CE-DGC.*

$m_{Al\text{-}salt}$ [g]	$m_{fumaric\ acid}$ [g]	n_{Al} [mmol]	$n_{fumaric\ acid}$ [mmol]	Yield [g]	Yield [%] [a]	BET [m^2g^{-1}]	Time [h]
0.159	0.111	0.48	0.96	0.0435	58	1284	6
0.157	0.109	0.47	0.94	0.0500	67	1037	6
0.159	0.111	0.48	0.96	0.0532	71	1129	24

[a] Based on the amount of Al-salt and on the product formula $[Al(OH)(O_2C\text{-}CH{=}CH\text{-}CO_2)]_n$ and M_W = 158.045 $gmol^{-1}$ for Alfum.

S5.3. Conventional solution-based synthesis

According to the patent by BASF,[57,58] we performed solution-based syntheses at 60 °C under aqueous reflux conditions in a round-bottom flask. Aluminum sulfate-octadecahydrate (1.1710 g, 1.76 mmol, 1 eq), sodium hydroxide (0.2803 g, 7.01 mmol, 4 eq) and fumaric acid (0.3863 g, 3.33 mmol, 2 eq) yielded 74% of product (0.4104 g; after vacuum, 80 °C, 24 h).

S6. PXRD measurements

Crystallinity and phase purity was examined with powder X-ray diffractometry (PXRD), using a *D2 Phaser* (BRUKER, Billerica, US) diffractometer with a flat silicon, low background sample holder and Cu-K_α radiation (λ = 1.54184 Å) at 30 kV and 0.04 °s^{-1} in the 2θ = 5-50 ° range. In the case of MIL-100(Fe) samples detector limits were 0.18 and 0.25 V, in order to suppress the X-ray-fluorescence of iron. Analyses of the diffractograms were carried out with *Match 3.11* software.

Relevant PXRD plots are given in the full paper.

S7. Nitrogen sorption experiments (T = 77 K)

Surface areas (BET) were determined by nitrogen (purity 99.999%, 5.0) sorption experiments at T = 77 K using a *NOVA-4000e* (QUANTACHROME, Odelzhausen, Germany) instrument within a partial pressure range of $p/p_0 = 10^{-3}$-1 bar. Each sample (20-50 mg each) was degassed under vacuum (< 10^{2} mbar) at 100 °C (MIL-100(Fe)), 120 °C (UiO-66, MIL-140A) and 150 °C (Alfum) for ca. 3 h, prior to measurement.

All surface areas (BET) were calculated from five adsorption points in the pressure range p/p_0 = 0.05-0.2 for samples of MIL-100(Fe), p/p_0 = 0.01-0.05 for UiO-66, p/p_0 = 0.01-0.10 for MIL-140A and p/p_0 = 0.001-0.05 for Alfum. This range is suitable for microporous materials.[58] Full isotherms were collected exemplarily and are given in the full paper in Fig. 2, Fig. 4 and Fig. 7.

Table S6 summarizes repeated N_2 sorption results of the industrial benchmarks *Basolite F300* and *Basolite A520* using the same batch, but not the same sample.

Table S6 *Repeated determination of BET surface areas of Basolite F300 and Basolite A520 using nitrogen sorption (T = 77 K).*

Benchmark	No. of measurement	BET [m^2 g^{-1}]
Basolite F300	1	1140
	2	1252
	3	847
	4	1100
	5	1024
Basolite A520	1	1030
	2	1038
	3	999
	4	1040
	5	1026

All relevant nitrogen isotherm plots are given in the full paper.

Figure S7 exemplarily depicts four N_2 sorption isotherms of Alfum obtained *via* MW-DGC, proving reproducibility of the composite Type I + Type IV isotherm, caused by micro-mesoporous structure (cf. Fig. S8 and S9).

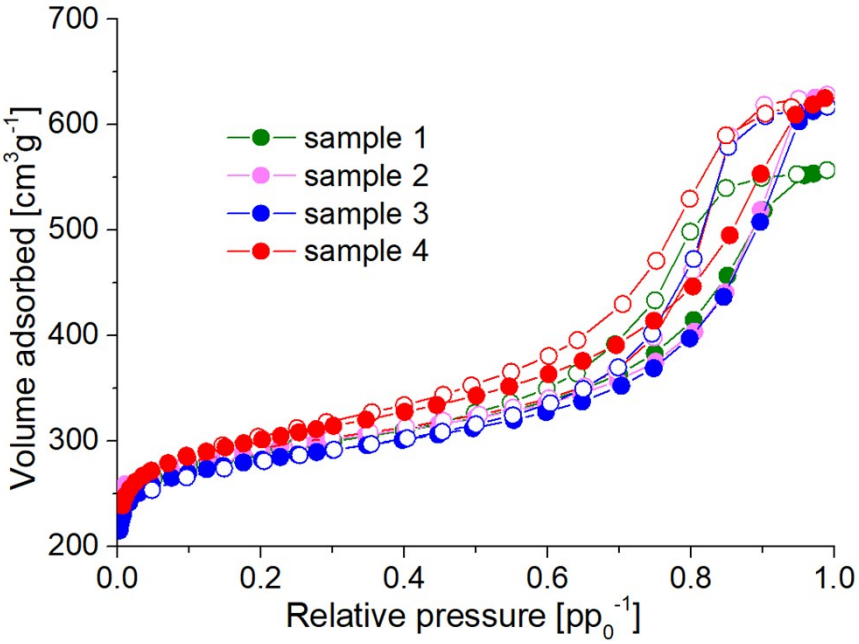

Figure S7 *Examples of nitrogen sorption isotherms (77 K) of four Alfum samples obtained via MW-DGC, revealing reproducibility of adsorption behavior, i.e. composite Type I + Type IV isotherm.*

S7.1. Pore size distributions of Alfum samples

Figures S8 and S9 depict the pore size distributions (NLDFT equilibrium model, carbon, slit pore, N_2 at 77 K) of Alfum samples obtained by different synthesis methods. All pore size distribution curves were calculated with the native *NovaWin 11.03* software using the 'N_2 at 77 K on carbon, slit pore, NLDFT equilibrium' model.

The images visualize the different porosity properties of Alfum samples obtained by different synthesis methods including *Basolite A520*.

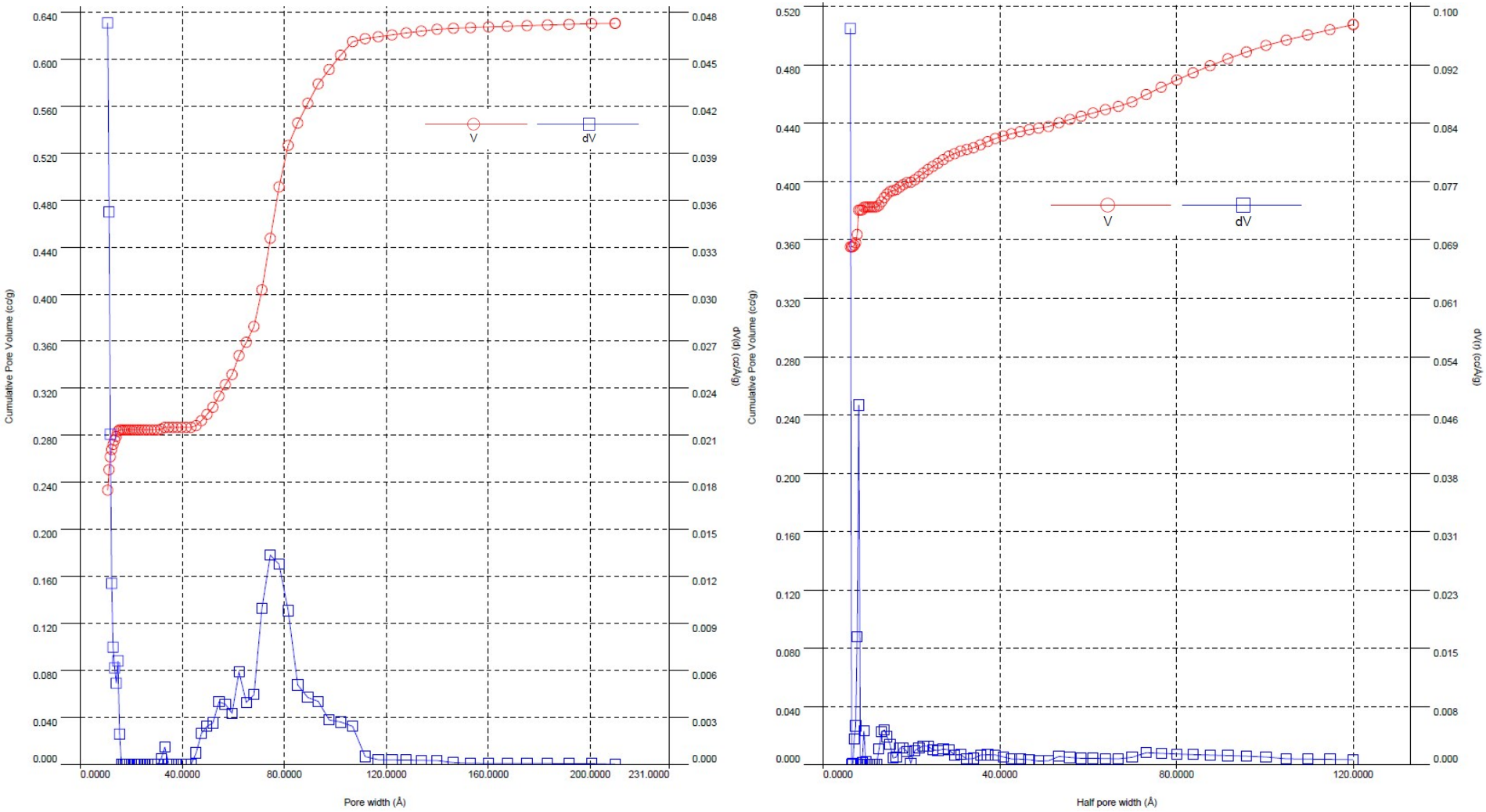

Figure S8 *Pore size distributions (NLDFT equilibrium model, carbon, slit pore, N_2 sorption at 77 K) of Alfum samples obtained by MW-DGC (left) and CE-DGC (right). The images shown here are representative examples out of more than 10 determined pore size distributions for the Alfum materials.*

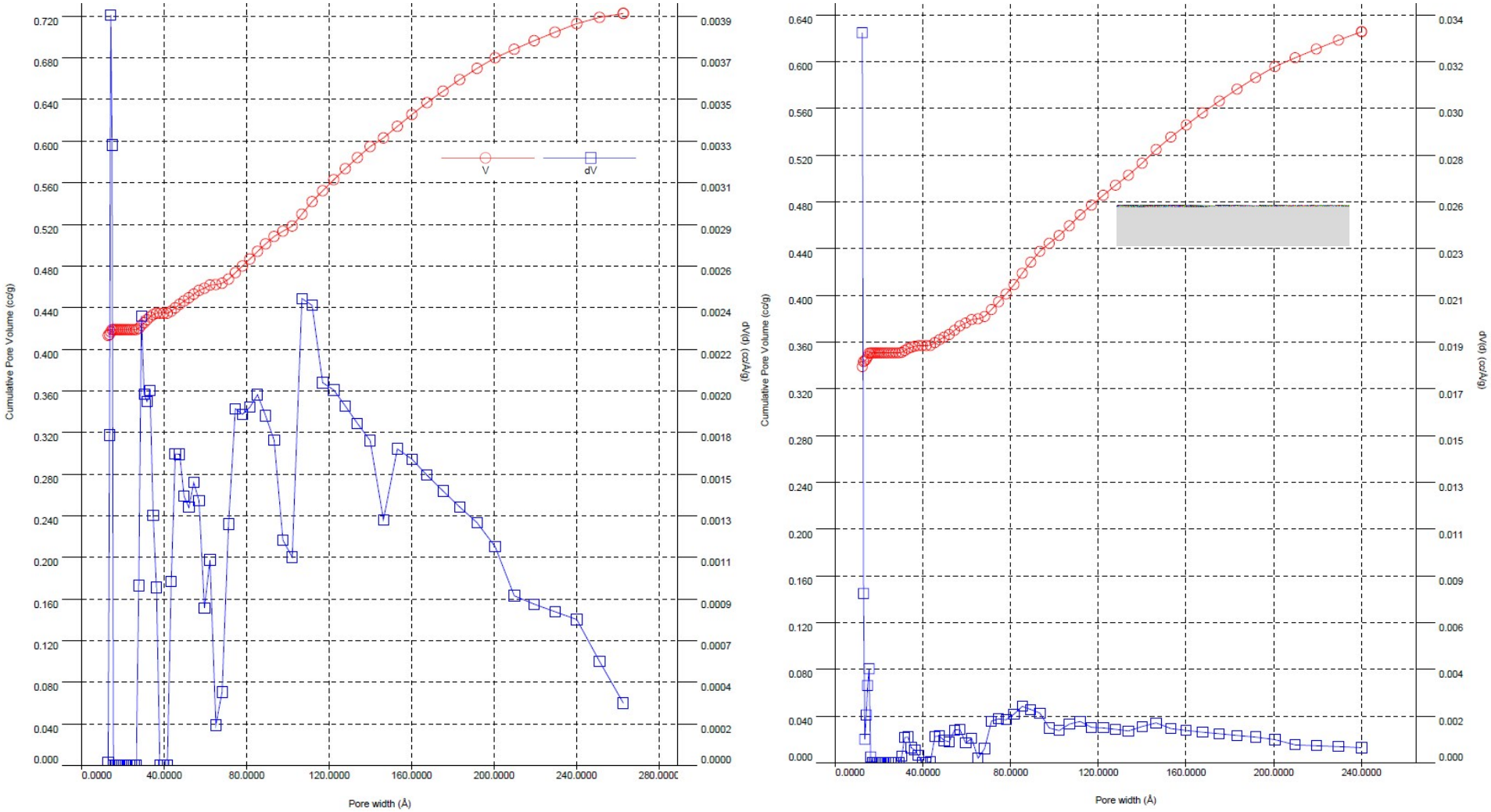

Figure S9 *Pore size distributions (NLDFT equilibrium model, carbon, slit pore, N_2 sorption at 77 K) of Alfum samples obtained by solution-based synthesis (left) and Basolite A520 (right). The images shown here are representative examples out of 6 determined pore size distributions for the Alfum materials.*

S7.2. Comparison of porosity parameters of Alfum samples

Table S7 summarizes the ranges from at least six samples from each synthesis method for Alfum within this work, described in Section S5. All values were derived from N_2 sorption isotherms using the native *NovaWin 11.03* software.

Table S7 *Ranges of porosity parameters from different Alfum samples obtained via MW-DGC, CE-DGC and solution-based synthesis in comparison with Basolite A520. At least six samples of each synthesis method were measured and taken into account.*

	S_{BET} [m^2g^{-1}] [a]	$S_{micro\text{-}BET}$ [m^2g^{-1}] [b]	S_{Ext} [m^2g^{-1}] [c]	$V_{pore\ (total)}$ [cm^3g^{-1}] [d]	$V_{pore\ (NLDFT)}$ [cm^3g^{-1}] [e]	$V_{pore\ (micro)}$ [cm^3g^{-1}] [f]
MW-DGC	1015-1148	781-912	216-307	0.67-0.96	0.72-0.94	0.27-0.36
CE-DGC	1037-1188	941-1089	86-118	0.43-0.72	0.43-0.61	0.37-0.42
Solution-based	780-1254	654-1120	126-134	0.49-0.72	0.36-0.72	0.26-0.43
Basolite A520	999-1040	885-930	109-114	0.58-0.63	0.51-0.63	0.31-0.36

[a] BET surface areas (S_{BET}) were obtained from five adsorption points in the pressure range pp_0^{-1}=0.001-0.05. [b] Micropore areas ($S_{micro\text{-}BET}$) were obtained by t-plot and V-t-method. [c] External area (S_{Ext}) refers to all area that does not originate from micropores and it includes meso- and macropores, i.e. pores > 2nm. Obtained by t-plot and V-t-method. [d] Total pore volumes ($V_{pore\ (total)}$) were derived at pp_0^{-1} = 0.95 for pores ≤20 nm. [e] Pore volumes from NLDFT ($V_{pore\ (NLDFT)}$) were calculated using 'N_2 at 77 K on carbon, slit pore, NLDFT equilibrium' model. [f] Micropore volume ($V_{pore\ (micro)}$) refers to volume that originates only from micropores, obtained by V-t-method with thickness method 'DeBoer'.
All correlation coefficients (r) within calculations were >0.999.

S8. Scanning electron microscopy (SEM)

The morphology was imaged by SEM using a *JSM-6510 advanced electron microscope* (JEOL, Akishima, Japan) with a LaB_6 cathode at 5-20 keV. Figures S10-S12 display obtained products at different scales.

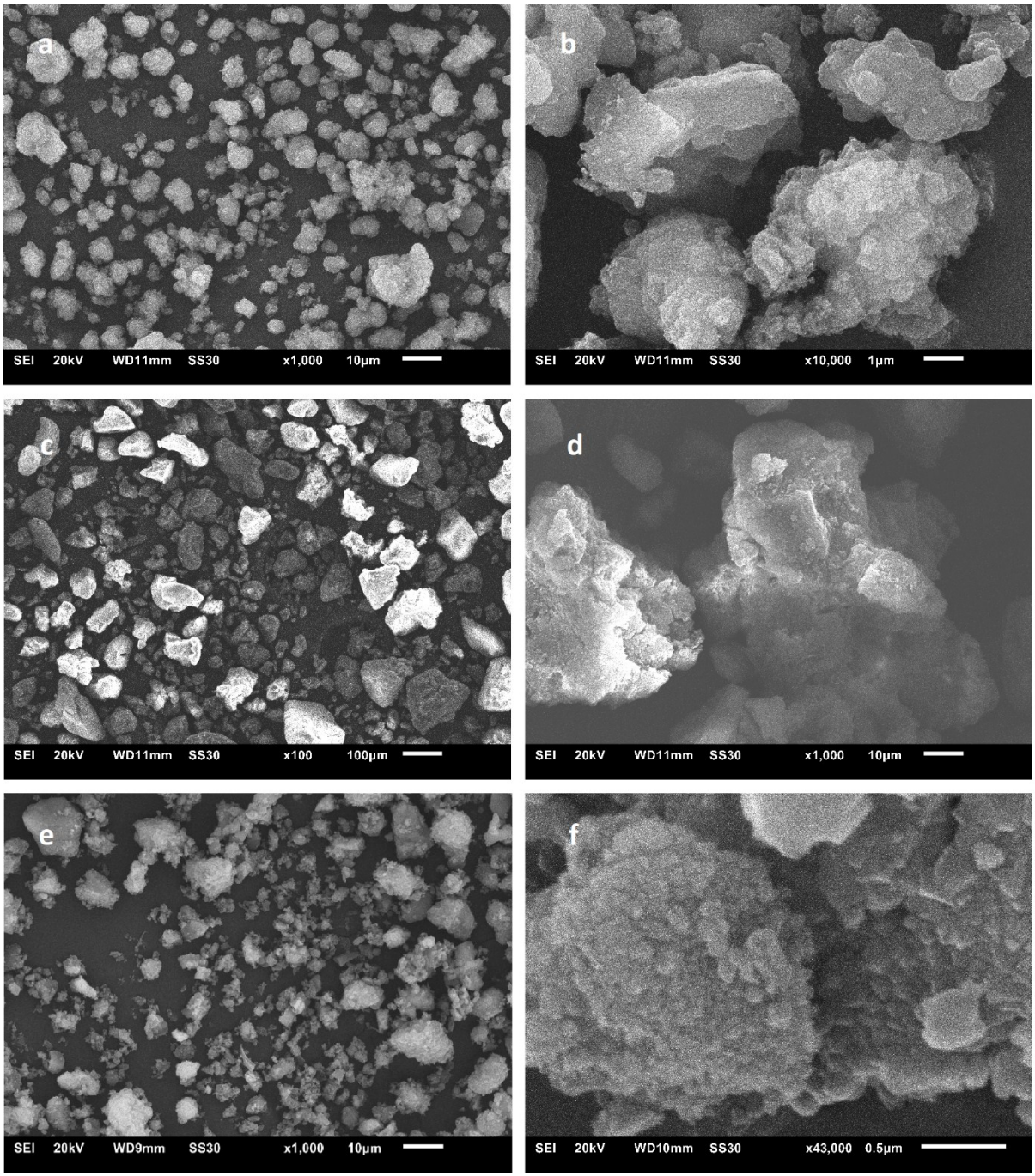

Figure S10 *SEM images of MIL-100(Fe) (left: overview, right: close-up): Basolite F300 (a, b), MW-DGC product (c, d) and CE-DGC product (e, f).*

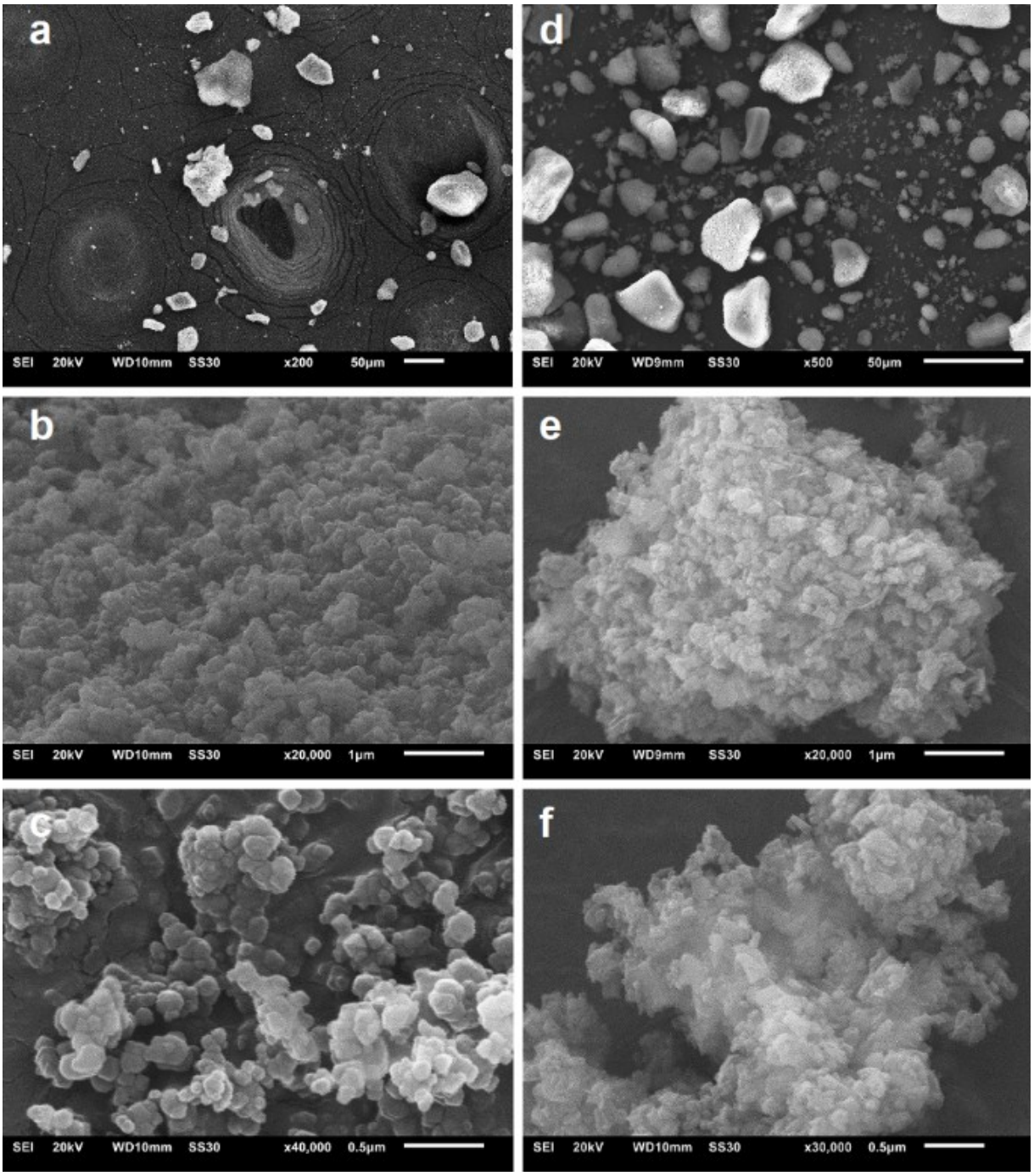

Figure S11 *SEM images of UiO-66-HCl (a, b and c) and MIL-140A (d, e and f) obtained via MW-DGC.*

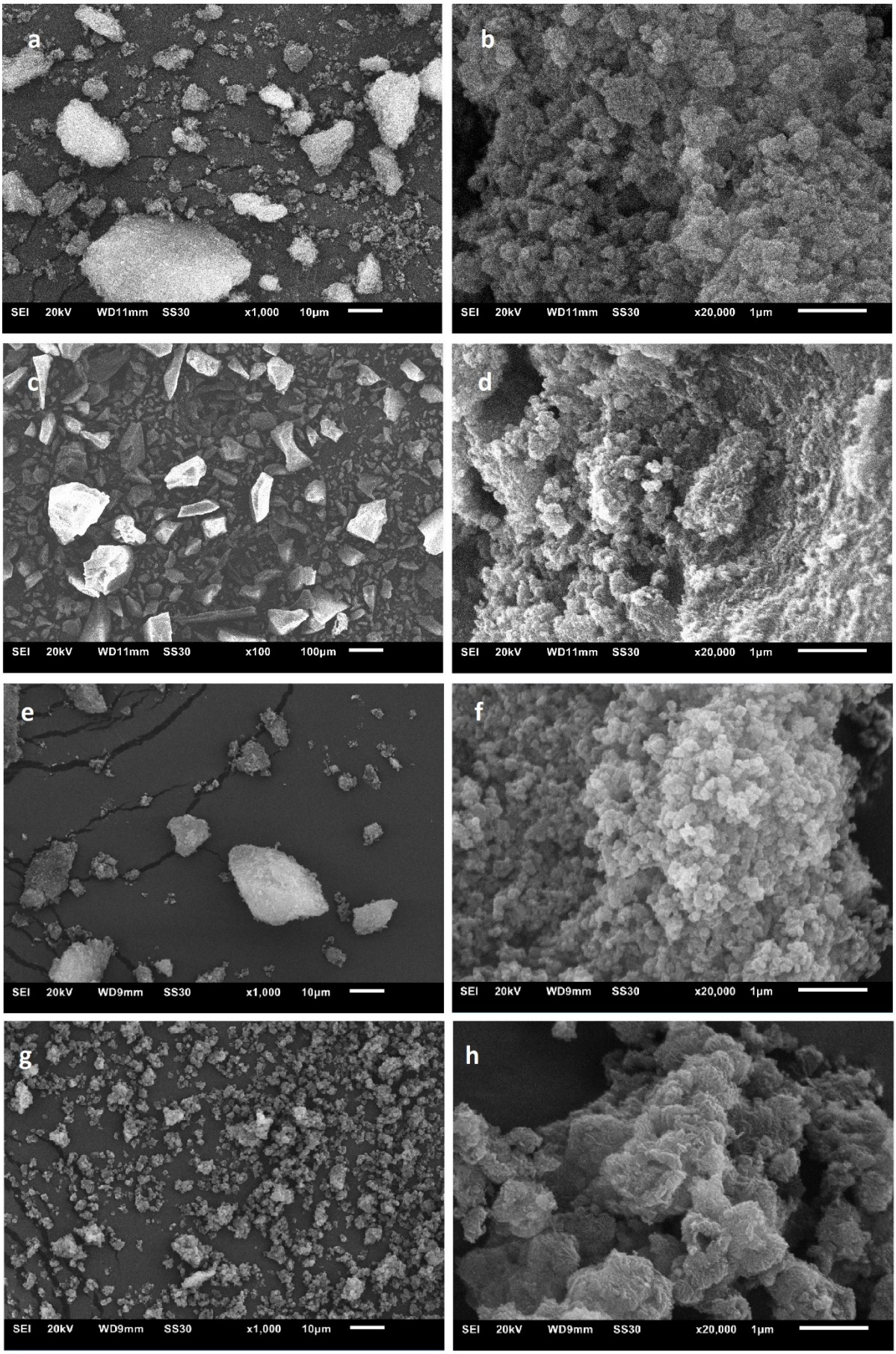

Figure S12 *SEM images of aluminum fumarate (left: overview, right: close-up): Basolite A520 (a, b), MW-DGC product (c, d), CE-DGC product (e, f) and conventional solution-based product (g, h).*

S9. Thermogravimetric Analysis (TGA)

TGA measurements were carried out on a *TG209 F3 Tarsus* (NETZSCH, Selb, Germany) device under synthetic air atmosphere, ramping with 5 $Kmin^{-1}$ to target temperature (600 °C).

Figure S13 shows the TGA curves of MW-DGC products of UiO-66 and MIL-140A in comparison to the CE-DGC product of UiO-66 from ref. 55.

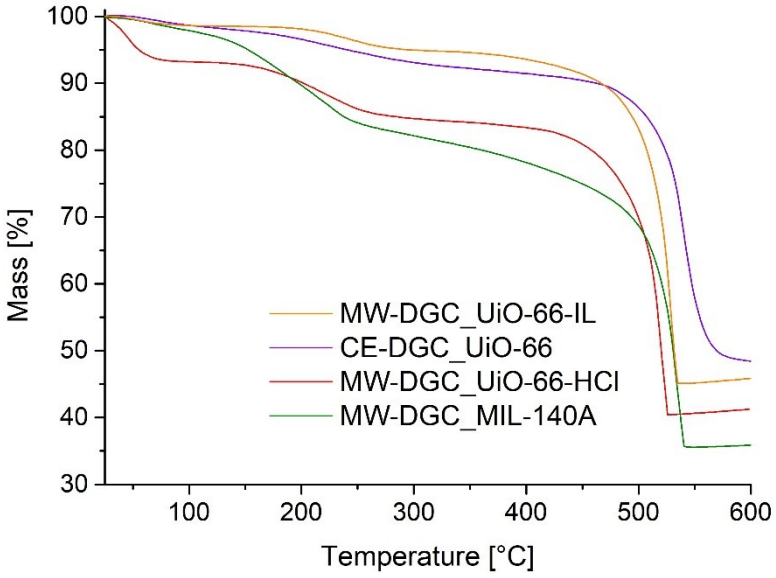

Figure S13 *TGA results of MW-DGC products UiO-66 and MIL-140A.*

Determination of defects per SBU was done similar to the procedure of Shearer *et. al.*.[43] An assumption of this method is that the residue in each TGA experiment is ZrO_2. The reaction of decomposition for both MOFs UiO-66 ($Zr_6O_6(BDC)_6$ (defect-free and dehydroxylated) and MIL-140A ZrO(BDC) can be described as follows:

$$Zr_6O_6(BDC)_6 + 45\ O_2 \longrightarrow 6\ ZrO_2 + 48\ CO_2 + 12\ H_2O$$

$$2\ ZrO(BDC) + 15\ O_2 \longrightarrow 2\ ZrO_2 + 16\ CO_2 + 4\ H_2O$$

The determination can be parted in three steps:

1) Determine the theoretical plateau weight $\mathbf{W_{Theo.Plat}}$:

$$W_{Theo.Plat} = (M_{Comp}/M_{6xZrO2}) \cdot W_{End}$$

$$W_{Theo.Plat} = (M_{Comp}/M_{ZrO2}) \cdot W_{End}$$

with M_{Comp} (UiO-66; dehydroxylated, defect-free) = 1628.03 g/mol, M_{Comp} (MIL-140A) = 271.22 g/mol, M_{6xZrO2} = 739.34 g/mol, M_{ZrO2} = 123.22 g/mol and W_{End} = 100%, which is the end weight of the TGA run (=normalized to 100%).

We obtain $W_{Theo.Plat}$ values of UiO-66 and MIL-140A:

$W_{Theo.Plat}$ (UiO-66) = 220.20%

$W_{Theo.Plat}$ (MIL-140A) = 220.20%

2) Determination of the weight contribution per BDC linker $\mathbf{Wt.PL_{Theo}}$:

$$Wt.PL_{Theo} = (W_{Theo.Plat} - W_{End})/NL_{Ideal}$$

$$Wt.PL_{Theo}\ (UiO\text{-}66) = (220.20-100)/6 = 20.03\%$$

$$Wt.PL_{Theo}\ (MIL\text{-}140A) = (220.20-100)/1 = 120.20\%$$

, while NL_{Ideal} is the number of linkers (1 or 6) in *ideal* Zr/Zr_6-SBU.

3) Calculation of number of linkers per *defective* Zr/Zr_6 unit $\mathbf{NL_{Exp}}$:

$$NL_{Exp} = (6\text{-}x) = (W_{Exp.Plat} - W_{End})/\ Wt.PL_{Theo} \text{ or } NL_{Exp} = (1\text{-}x) = (W_{Exp.Plat} - W_{End})/\ Wt.PL_{Theo}$$

, while $W_{Exp.Plat}$ is the experimental TGA plateau. The value can be taken from **Figure S*13***. $\boldsymbol{x}$ is the number of linker deficiencies per Zr_6 SBU. We used following equations to calculate:

$$x = 6 - NL_{Exp} = 6\text{-}[(W_{Exp.Plat} - W_{End})/Wt.PL_{Theo}]$$

$$x = 1 - NL_{Exp} = 1\text{-}[(W_{Exp.Plat} - W_{End})/Wt.PL_{Theo}]$$

x (CE-DGC-UiO-66) = 6−4.643 = 6−((**193.0**−100%)/20.03%) = **1.357 ≅ 1.36** [55]

x (MW-DGC-UiO-66-HCl) = 6−4.833 = 6−((**196.8**−100%)/20.03%) = **1.167 ≅ 1.17**

x (MW-DGC-UiO-66-IL) = 6−4.843 = 6−((**197.0**−100%)/20.03%) = **1.157 ≅ 1.16**

x (MW-DGC-MIL-140A) = 1−0.970 = 1−((**216.5**−100%)/120.2%) **≅ 0.03**

S10. Results of three synthesis runs with solvent re-use

The MW-DGC synthesis procedures described in Section S3 were exemplarily performed with solvent re-use, that is, using the same solvent, but fresh precursor on top of the DGC sieve each time.

Figures S14-S17 show PXRD patterns of all four presented MOFs, each proving maintaining crystallinity over three repeated synthesis runs with solvent re-use.

According to the data given in the Tables S8-S11 (cf. Fig. 8 in the full manuscript), we were able to prove the re-use of solvent with good yields and high specific surface areas (BET).

S10.1 MIL-100(Fe)

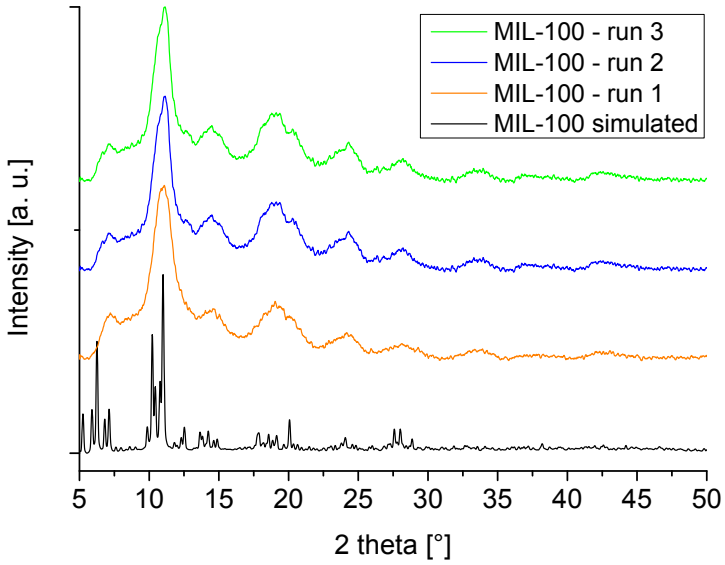

Figure S14 *PXRD patterns of MIL-100(Fe) samples from repeated synthesis runs with solvent re-use.*

Table S8 *Results of three repeated synthesis runs with re-use of solvent for MIL-100(Fe).*

Run	BET [m^2g^{-1}]	Yield [%]
1	1287	78
2	935	72
3	1158	82

S10.2. UiO-66-IL

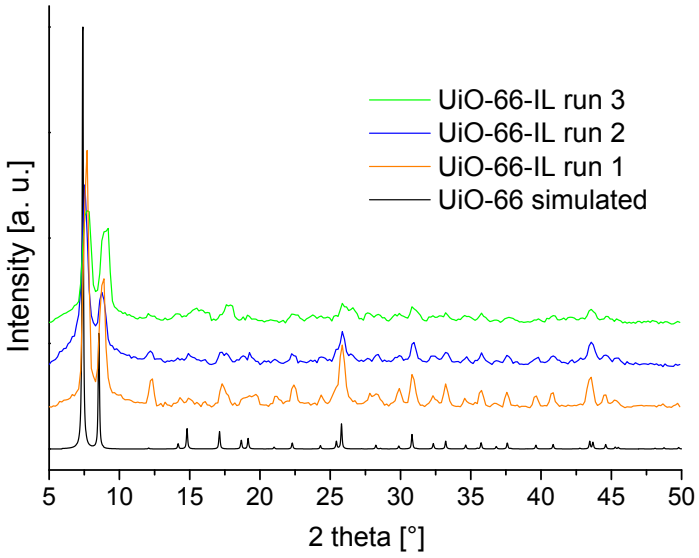

Figure S15 *PXRD patterns of UiO-66-IL samples from repeated synthesis runs with solvent re-use.*

Table S9 *Results of three repeated synthesis runs with re-use of solvent for UiO-66-IL.*

Run	BET [m^2g^{-1}]	Yield [%]
1	1023	68
2	807	73
3	717	72

S10.3. MIL-140A

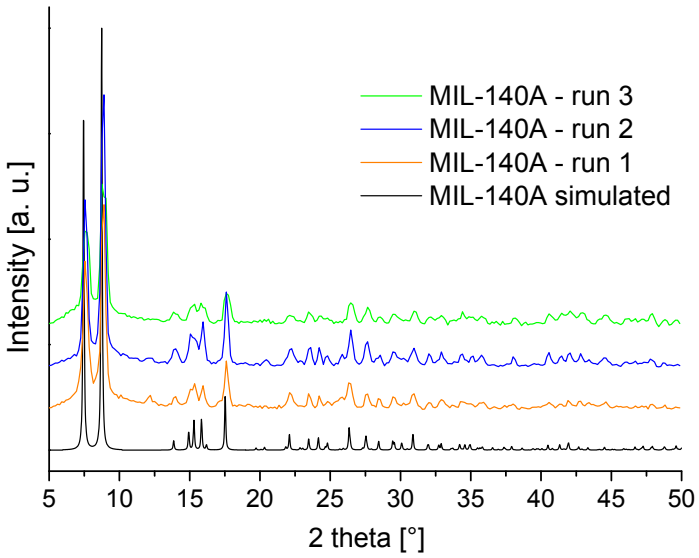

Figure S16 *PXRD patterns of MIL-140A samples from repeated synthesis runs with solvent re-use.*

Table S10 *Results of three repeated synthesis runs with re-use of solvent for MIL-140A.*

Run	BET [m^2g^{-1}]	Yield [%]
1	354	92
2	340	89
3	344	96

S10.4. Aluminum fumarate

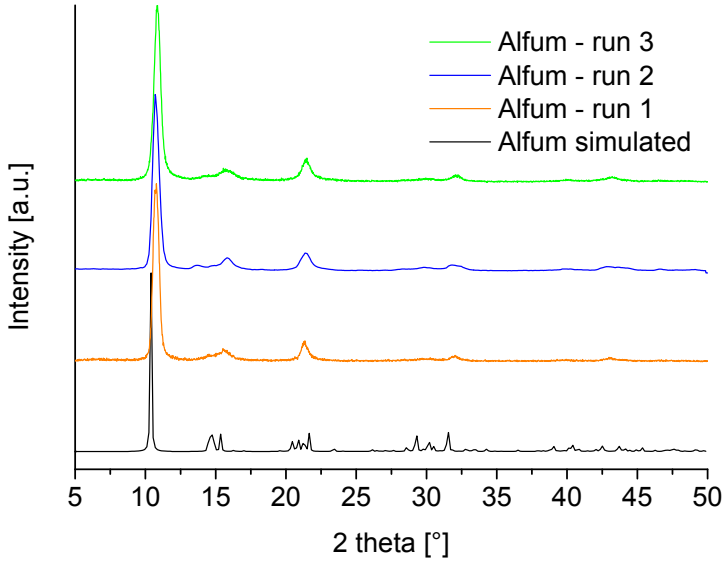

Figure S17 *PXRD patterns of Alfum samples from repeated synthesis runs with solvent re-use.*

Table S11 *Results of three repeated synthesis runs with re-use of solvent for aluminum fumarate.*

Run	BET [m^2g^{-1}]	Yield [%]
1	1075	76
2	1148	81
3	1128	89

S11. Calculation of solvent amounts

- for aluminum fumarate

The patented synthesis procedure for continuous production of Alfum demonstrates different methods with varying STYs from 2032-5339 kg m^{-3} day^{-1}. The most effective one (i.e. 3615 kg m^{-3} day^{-1}) yields 97.5 mol-% based on Al, achieving 4.1 wt.% product in solution.[57]

3615 kg m^{-3} day^{-1} = 4.1 wt.% of product in solution

→ 95.9 wt.% mother liquor = 84555.73 kg = 84.55 tons

- for UiO-66

The continuous flow synthesis procedure reports STY = 7163 kg m^{-3} day^{-1} with a concentration of 0.1 mol L^{-1} Zr in solution, 94% yield (i.e. 0.094 mol L^{-1} product in solution), a flow of 1.23 mL min^{-1}.
Specifically it is stated that from 20 mL processed a yield of 0.696 g (94%)" of desolvated MOF in 24.4 min total run time was obtained.
This amounts to 0.696 g / [(0.020 L/10^{-3} L/m^3) x (24.4 min/1440 min/day)] = 2054 kg m^{-3} day^{-1}.

There is an additional solvent amount of 8 mL + 10 mL and 60 mL for washing, that is in total apparently 98 mL for the STY of 2053 kg m^{-3} day^{-1}

From only the 20 mL = 0.02 L and STY of 2054 kg m^{-3} day^{-1} the solvent volume per day is estimated as

$$x = 2053 \cdot 10^3 \text{ g} / 0.696 \text{ g} \times 0.02 \text{ L} = \underline{59\,000 \text{ L}}$$

From the total of 98 mL = 0.098 L and STY of 2054 kg m^{-3} day^{-1} the solvent volume per day is estimated:

$$x = 2053 \cdot 10^3 \text{ g} / 0.696 \text{ g} \times 0.098 \text{ L} = \underline{289\,000 \text{ L}}$$

S12. References

1 G. Férey, C. Serre, C. Mellot-Draznieks, F. Millange, S. Surblé, J. Dutour and I. Margiolaki, *Angew. Chem.*, 2004, **116**, 6456-6461.

2 K. Brandenburg, Diamond 4.3.1, Crystal and Molecular Structure Visualization, Crystal Impact - K. Brandenburg & H. Putz GbR, Bonn, Germany, 2009.

3 P. Horcajada, S. Surblé, C. Serre, D.-Y. Hong, Y.-K. Seo, J.-S. Chang, J.-M. Grèneche, I. Margiolaki and G. Férey, *Chem. Commun.*, 2007, **27**, 2820-2822.

4 L. Sciortino, A. Alessi, F. Messina, G. Buscarino and F. M. Gelardi, *J. Phys. Chem. C*, 2015, **119**, 7826-7830.

5 F. Jeremias, S. K. Henninger and C. Janiak, *Dalton Trans.*, 2016, **45**, 8637-8644.

6 J. W. Yoon, Y.-K. Seo, Y. K. Hwang, J.-S. Chang, H. Leclerc, S. Wuttke, P. Bazin, A. Vimont, M. Daturi, E. Bloch P. L. Llewellyn, C. Serre, P. Horcajada, J.-M. Grenèche, A. E. Rodrigues and G. Férey, *Angew. Chem.*, 2010, **122**, 6085-6088.

7 P. L. Llewellyn, S. Bourrelly, C. Serre, A. Vimont, M. Daturi, L. Hamon, G. de Weireld, J.-S. Chang, D.-Y. Hong, Y. K. S. H. Jhung and G. Férey, *Langmuir*, 2008, **24**, 7245-7250.

8 I. Ahmed and S. H. Jhung, *Mater. Today*, 2014, **17,** 136-146.

9 C. Petit and T. J. Bandosz, *Adv. Funct. Mater.*, 2011, **21**, 2108-2117.

10 F. Jeremias, A. Khutia, S. K. Henninger and C. Janiak, *J. Mater. Chem.*, 2012, **22**, 10148-10151.

11 S. K. Henninger, F. Jeremias, H. Kummer, P. Schossig and H.-M. Henning, *Energy Proced.*, 2012, **30**, 279-288.

12 S. K. Henninger, F. Jeremias, H. Kummer and C. Janiak, *Eur. J. Inorg. Chem.*, 2012, **16**, 2625-2634.

13 A. Rezk, R. Al-Dadah, S. Mahmoud and A. Elsayed, *Int. J. Heat Mass Tran.*, 2012, **55**, 7366-7374.

14 S. Kovačič, M. Mazaj, M. Ješelnik, D. Pahovnik, E. Žagar, C. Slugovc and N. Z. Logar, *Macromol. Rapid Comm.*, 2015, **36**, 1605-1611.

15 A. G. Márquez, A. Demessence, A. E. Platero-Prats, D. Heurtaux, P. Horcajada, C. Serre, J.-S. Chang, G. Férey, V. A. de la Peña-O'Shea, C. Boissière, D. Grosso and C. Sanchez, *Eur. J. Inorg. Chem.*, 2012, 5165-5174.

16 M. Pilloni, F. Padella, G. Ennas, S. Lai, M. Bellusci, E. Rombi, F. Sini, M. Pentimalli, C. Delitala, A. Scano, V. Cabras and I. Ferino, *Micropor. Mesopor. Mater.*, 2015, **213**, 14-21.

17 S. Rojas, F. J. Carmona, C. R. Maldonado, E. Barea and J. A. R. Navarro, *New J. Chem.*, 2016, **40**, 5690-5694.

18 E. Bellido, M. Guillevic, T. Hidalgo, M. J. Santander-Ortega, C. Serre and P. Horcajada, *Langmuir*, 2014, **30**, 5911-5920.

19 A. García Márquez, A. Demessence, A. E. Platero-Prats, D. Heurtaux, P. Horcajada, C. Serre, J.-S. Chang, G. Férey, de la Peña-O'Shea, Victor Antonio, C. Boissière, D. Grosso and C. Sanchez, *Eur. J. Inorg. Chem.*, 2012, 5165-5174.

20 F. Tan, M. Liu, K. Li, Y. Wang, J. Wang, X. Guo, G. Zhang and C. Song, *Chem. Eng. J.*, 2015, **281**, 360-367.

21 L. Li, S. Xiang, S. Cao, J. Zhang, G. Ouyang, L. Chen and C.-Y. Su, *Nat. Commun.*, 2013, **4**, article

number 1774.
22 B. Zhang, J. Zhang, C. Liu, L. Peng, X. Sang, B. Han, X. Ma, T. Luo, X. Tan and G. Yang, *Sci. Rep.*, 2016, **6**, article number 21401.
23 F. Vermoortele, R. Ameloot, L. Alaerts, R. Matthessen, B. Carlier, E. V. R. Fernandez, J. Gascon, F. Kapteijn and D. E. de Vos, *J. Mater. Chem.*, 2012, **22**, 10313-10321.
24 J.-W. Zhang, G.-P. Lu and C. Cai, *Green Chem.*, 2017, **19**, 4538-4543.
25 A. U. Czaja, N. Trukhan and U. Müller, *Chem. Soc. Rev.*, 2009, **38**, 1284-1293.
26 M. Rubio-Martinez, T. D. Hadley, M. P. Batten, K. Constanti-Carey, T. Barton, D. Marley, A. Mönch, K.-S. Lim and M. R. Hill, *ChemSusChem*, 2016, **9**, 938-941.
27 M. Rubio-Martinez, C. Avci-Camur, A. W. Thornton, I. Imaz, D. Maspoch and M. R. Hill, *Chem. Soc. Rev.*, 2017, **46**, 3453-3480.
28 M. J. Katz, Z. J. Brown, Y. J. Colón, P. W. Siu, K. A. Scheidt, R. Q. Snurr, J. T. Hupp and O. K. Farha, *Chem. Commun*., 2013, **49**, 9449-9451.
29 G. C. Shearer, S. Chavan, S. Bordiga, S. Svelle, U. Olsbye and K. P. Lillerud, *Chem. Mater.*, 2016, **28**, 3749-3761.
30 J. H. Cavka, S. Jakobsen, U. Olsbye, N. Guillou, C. Lamberti, S. Bordiga and K.P. Lillerud, *J. Am. Chem. Soc.*, 2008, **130**, 13850-13851.
31 V. Guillerm, F. Ragon, M. Dan-Hardi, T. Devic, M. Vishnuvarthan, B. Campo, A. Vimont, G. Clet, Q. Yang, G. Maurin, G. Férey, A. Vittadini, S. Gross and C. Serre, *Angew. Chem. Int. Ed.*, 2012, **51**, 9267-9271.
32 L. Valenzano, B. Civalleri, S. Chavan, S. Bordiga, M. H. Nilsen, S. Jakobsen, K. P. Lillerud and C. Lamberti, *Chem. Mater.*, 2011, **23**, 1700-1718.
33 H. Wu, Y. S. Chua, V. Krungleviciute, M. Tyagi, P. Chen, T. Yildirim and W. Zhou, *J. Am. Chem. Soc.*, 2013, **135**, 10525-10532.
34 M. W. Anjum, F. Vermoortele, A. L. Khan, B. Bueken, D. E. De Vos and I. F. J. Vankelecom, *ACS Appl. Mater. Interfaces*, 2015, **7**, 25193-25201.
35 F. Jeremias, V. Lozan, S. K. Henninger and C. Janiak, *Dalton Trans.,* 2013, **42**, 15967-15973.
36 F. Jeremias, D. Fröhlich, C. Janiak and S. Henninger, *New J. Chem.*, 2014, **38**, 1846-1852.
37 A. Shahat H. M. A. Hassan and H. M. E. Azzazy, *Analyt. Chim. Acta*, 2013, **793**, 90-98.
38 F. Vermoortele, B. Bueken, G. Le Bars, B. Van de Voorde, M. Vandichel, K. Houthoofd, A. Vimont, M. Daturi, M. Waroquier, V. Van Speybroeck, C. Kirschhock and D. E. De Vos, *J. Am. Chem. Soc.*, 2013, **135**, 11465-11468.
39 W. Cao, W. Luo, H. Ge, Y. Su, A. Wang and T. Zhang, *Green Chem.*, 2017, **19**, 2201-2211.
40 K. Užarević, T. C. Wang, S.-Y. Moon, A. M. Fidelli, J. T. Hupp, O. K. Farha and T. Friščić, *Chem. Commun.*, 2016, **52**, 2133-2136.
41 S. Gökpinar, T. Diment and C. Janiak, *Dalton Trans.*, 2017, **46**, 9895-9900.
42 M. Taddei, D. A. Steitz, J. A. van Bokhoven and M. Ranocchiari, *Chem. Eur. J.*, 2016, **22**, 3245-3249.
43 E. Leung, U. Müller, N. Trukhan, H. Mattenheimer, G. Cox and S. Blei, *Process for preparing porous metal-organic frameworks based on aluminum fumarate*, U.S. Patent No. 8,524,932, BASF SE, 3 Sep. 2013.
44 C. Kiener, U. Müller and M. Schubert, *Method of using a metal organic frameworks based on aluminum fumarate*, U.S. Patent No. 8,518,264, BASF SE, 27 Aug. 2013.
45 F. Jeremias, D. Fröhlich, C. Janiak and S. K. Henninger, *RSC Adv.*, 2014, **4**, 24073-24082.
46 E. Alvarez, N. Guillou, C. Martineau, B. Bueken, B. Van de Voorde, C. Le Guillouzer, P. Fabry, F. Nouar, F. Taulelle, D. de Vos, J.-S. Chang, K. H. Cho, N. Ramsahye, T. Devic, M. Daturi, G. Maurin and C. Serre, *Angew. Chem. Int. Ed.*, 2015, **54**, 3664-3668.
47 T. Loiseau, C. Volkringer, M. Haouas, F. Taulelle and G. Férey, *C. R. Chim.*, 2015, **18**, 1350-1369.
48 B. Yilmaz, N. Trukhan and U. Müller, *Chin. J. Catal.*, 2012, **33**, 3-10.
49 J. Chen, K. Shen and Y. Li, *ChemSusChem*, 2017, **10**, 3165-3187.
50 M. Gaab, N. Trukhan, S. Maurer, R. Gummaraju and U. Müller, *Micropor. Mesopor. Mater.*, 2012, **157**, 131-136.
51 S. Karmakar, J. Dechnik, C. Janiak and S. De, *J. Hazard. Mater.*, 2016, **303**, 10-20.

52 E. Elsayed, R. Al-Dadah, S. Mahmoud, P. A. Anderson, A. Elsayed and P. G. Youssef, *Desalination*, 2017, **406**, 25-36.
53 P. G. Yot, L. Vanduyfhuys, E. Alvarez, J. Rodriguez, J.-P. Itié, P. Fabry, N. Guillou, T. Devic, I. Beurroies, P. L. Llewellyn V. Van Speybroek, C. Serre and G. Maurin, *Chem. Sci.*, 2016, **7**, 446-450.
54 D. E. Crawford and J. Casaban, *Adv. Mater.*, 2016, **28**, 5747-5754.
55 D. Crawford, J. Casaban, R. Haydon, N. Giri, T. McNally and S. L. James, *Chem. Sci.*, 2015, **6**, 1645-1649.
56 M. Deetlefs and K. R. Seddon, *Green Chem.*, 2003, **5**, 181-186.
57 S. Wegner, C. Rutz, K. Schette, J. Barthel and A. Bushmelev, *Chem. Eur. J.*, 2017, **23**, 6330-6340.
58 M. Thommes, K. Kaneko, A. V. Neimark, J. P. Olivier, F. Rodriguez-Reinoso, J. Rouquerol and K. S. Sing, *Pure Appl. Chem.*, 2015, **87**, 1051-1069.